Supporting Information for

Synthesis, Characterization, and Water Adsorption Properties of a Novel Multi-Walled Carbon Nanotube/ MIL-100(Fe) Composite

Najam ul Qadir,[†] Syed A. M. Said,[†,‡,*] Rached Ben Mansour,[†,‡] Khalid Mezghani,[‡] Anwar-ul-Hamid[#]

[†]Center of Research Excellence in Renewable Energy, King Fahd University of Petroleum and Minerals, Dhahran 31261, Kingdom of Saudi Arabia

[‡]Center of Carbon Capture and Sequestration, King Fahd University of Petroleum and Minerals, Dhahran 31261, Kingdom of Saudi Arabia

[#]Center of Engineering Research, King Fahd University of Petroleum and Minerals, Dhahran 31261, Kingdom of Saudi Arabia

*To whom correspondence should be addressed: Email: samsaid@kfupm.edu.sa

Table of Contents

Section	Page(s)
Wt.% of MWCNTs in MWCNT/MIL-100(Fe) composites	1–2
Magnified SEM images of MIL-100(Fe) and MWCNT/MIL-100(Fe) composites	2–4
Magnified TEM images of MIL-100(Fe) and MWCNT/MIL-100(Fe) composites	5
PXRD patterns of pristine and functionalized MWCNTs	6
FTIR spectra of pristine and functionalized MWCNTs	6
Step-wise synthesis of MWCNT/MIL-100(Fe) composite	7
Magnified FTIR spectra of MIL-100(Fe) and MWCNT/MIL-100(Fe) composites	8
XPS spectra of acid-treated MWCNTs, MIL-100(Fe) and MC3	9–10
SEM micrographs of pristine and acid-treated (functionalized) MWCNTs	11
EDS analysis of MIL-100(Fe) and MWCNT/MIL-100(Fe) composites	12–13
PXRD patterns of iron oxide (α-Fe_2O_3) residues recovered after TGA of MIL-100(Fe) and MWCNT/MIL-100(Fe) composites	13
TGA of acid-treated MWCNTs in air	14
Calculation of specific heat capacity using DSC data	14
Comparison of adsorption isotherms at 298 and 313 K	15
Calculation of differential isosteric heat of adsorption	15–16
Power capability for MIL-100(Fe) and MWCNT/MIL-100(Fe) composites	17
Correlation between desorption behavior and isosteric heat of adsorption	18
SEM micrograph comparison before and after cyclic adsorption/desorption	19
PXRD profile comparison before and after cyclic adsorption/desorption	20
Supporting Information References	21

1. Calculation of weight percentage of MWCNTs in MWCNT/MIL-100(Fe) composites

The content of MWCNTs in the MWCNT/MIL-100(Fe) composites can be calculated using the TGA data using Eq. (S1):

$$\mathbf{MWCNTs\,(wt.\%)} = \left[\mathbf{W.L.}^{\mathbf{comp}}_{\mathbf{T_{MWCNTs-O_2}\rightarrow 700^oC}} - \mathbf{W.L.}^{\mathbf{MIL-100(Fe)}}_{\mathbf{353^oC\rightarrow 700^oC}}\right] + \mathbf{0.75} \quad \text{(S1)}$$

where $\mathbf{T_{MWCNTs-O_2}}$ is the temperature at which linker decomposition ends or MWCNT oxidation begins during TGA, $\mathbf{W.L.}^{\mathbf{comp}}_{\mathbf{T_{MWCNTs-O_2}\rightarrow 700\,^oC}} = \mathbf{W}^{\mathbf{comp}}_{\mathbf{T_{MWCNTs-O_2}}} - \mathbf{W}^{\mathbf{comp}}_{\mathbf{700\,^oC}}$ stands for the weight loss between $\mathbf{T_{MWCNTs-O_2}}$ and 700 ^{o}C expressed as a percentage of the initial weight, and the superscript "comp" denotes MWCNT/MIL-100(Fe) composite. For MIL-100(Fe), the linker decomposition was observed to end at 353 ^{o}C from the TGA profile. The weight loss for MIL-100(Fe) between 353 and 700 ^{o}C was measured to be equal to 1.8148 wt%, i.e. $\mathbf{W.L.}^{\mathbf{MIL-100(Fe)}}_{\mathbf{353\,^oC\rightarrow 700\,^oC}} = 1.8148\%$. The residual MWCNTs at the end of TGA amount to 0.75 wt%. The corresponding percentages of MWCNTs in the composites are calculated to be 2.16, 5.90 and 10.72, respectively. The synthesized MWCNT/MIL-100(Fe) composites are referred to as MC*n* with *n* from 1 to 3 corresponding to the amount of added MWCNTs (60 mg, 180 mg and 300 mg respectively).

Table S1. Calculation of weight percentages of MWCNTs in MWCNT/MIL-100(Fe) composites using TGA data.

Sample ID	$T_{MWCNTs\text{-}O_2}$ (°C)	$W^{comp}_{T_{MWCNTs\text{-}O_2}}$ (%)	$W^{comp}_{700^oC}$ (%)	$W.L.^{comp}_{T_{MWCNTs\text{-}O_2}\rightarrow 700^oC}$	MWCNTs (wt%)
MC1	350	62.5031	59.2829	3.2202	2.1587
MC2	345	55.9593	48.9947	6.9647	5.9032
MC3	333	57.4979	45.7181	11.7799	10.7184

2. Magnified SEM images of MIL-100(Fe) and MWCNT/MIL-100(Fe) composites

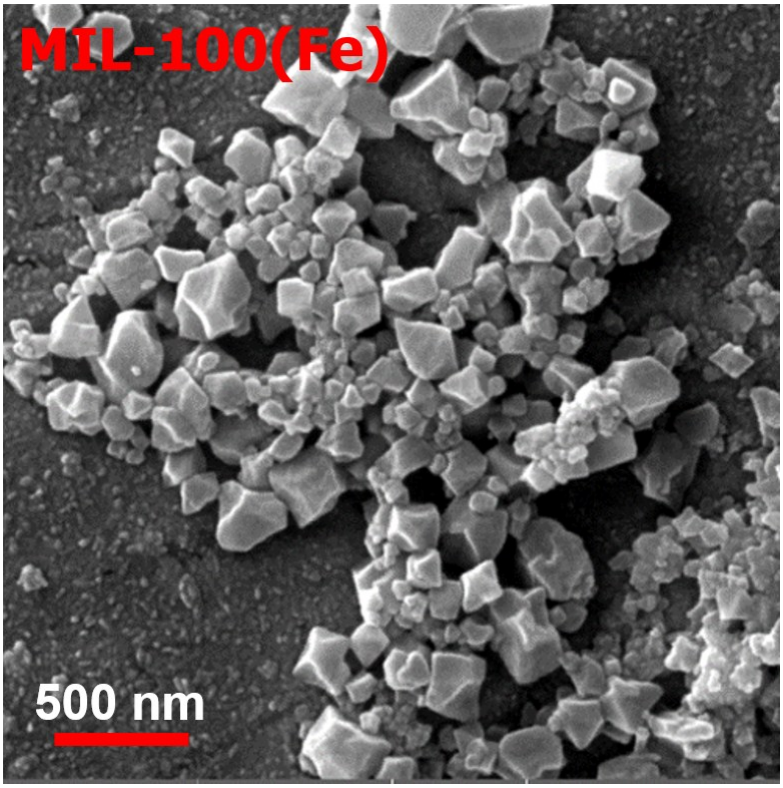

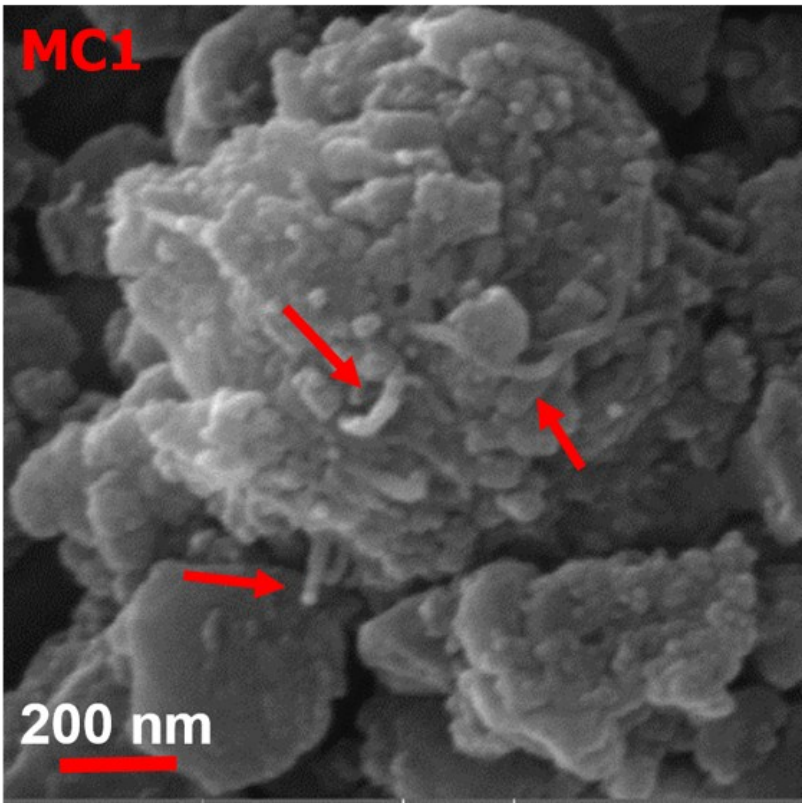
MC1
200 nm

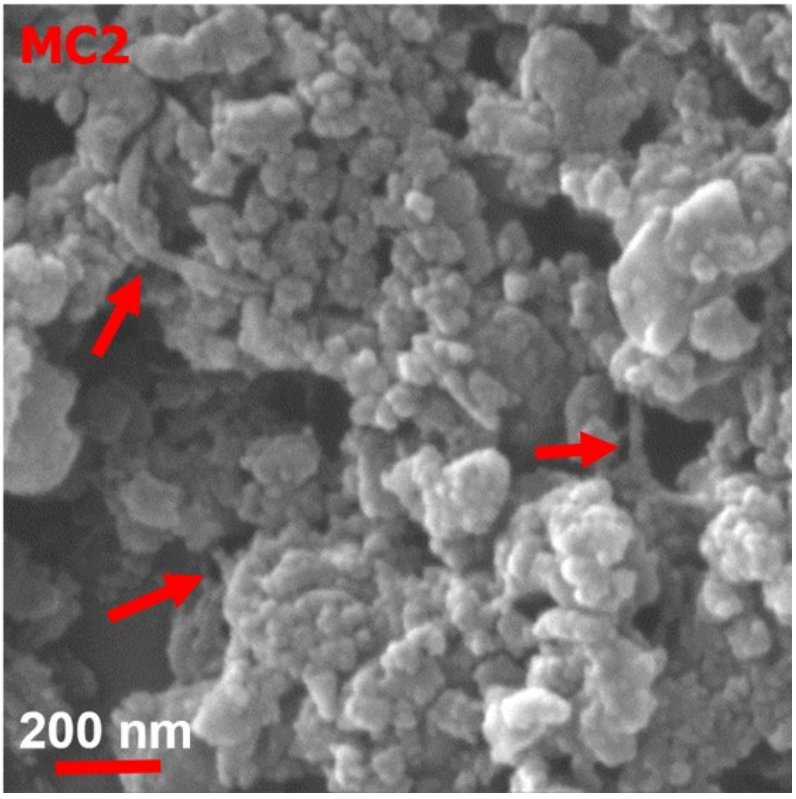
MC2
200 nm

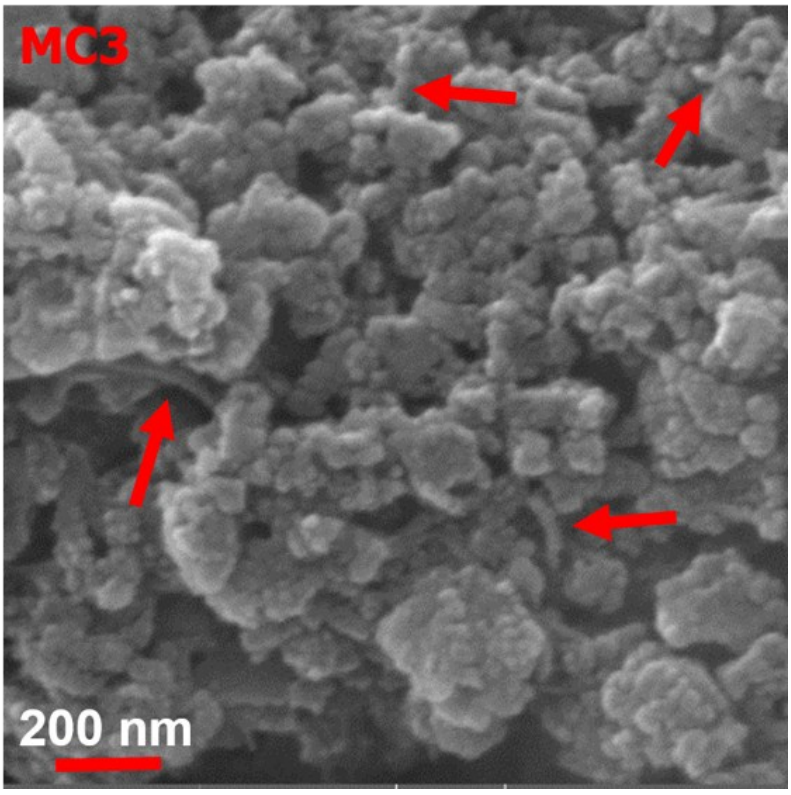

Red arrows indicate locations of MWCNTs.

3. **Magnified TEM images of MIL-100(Fe) and MWCNT/MIL-100(Fe) composite.**

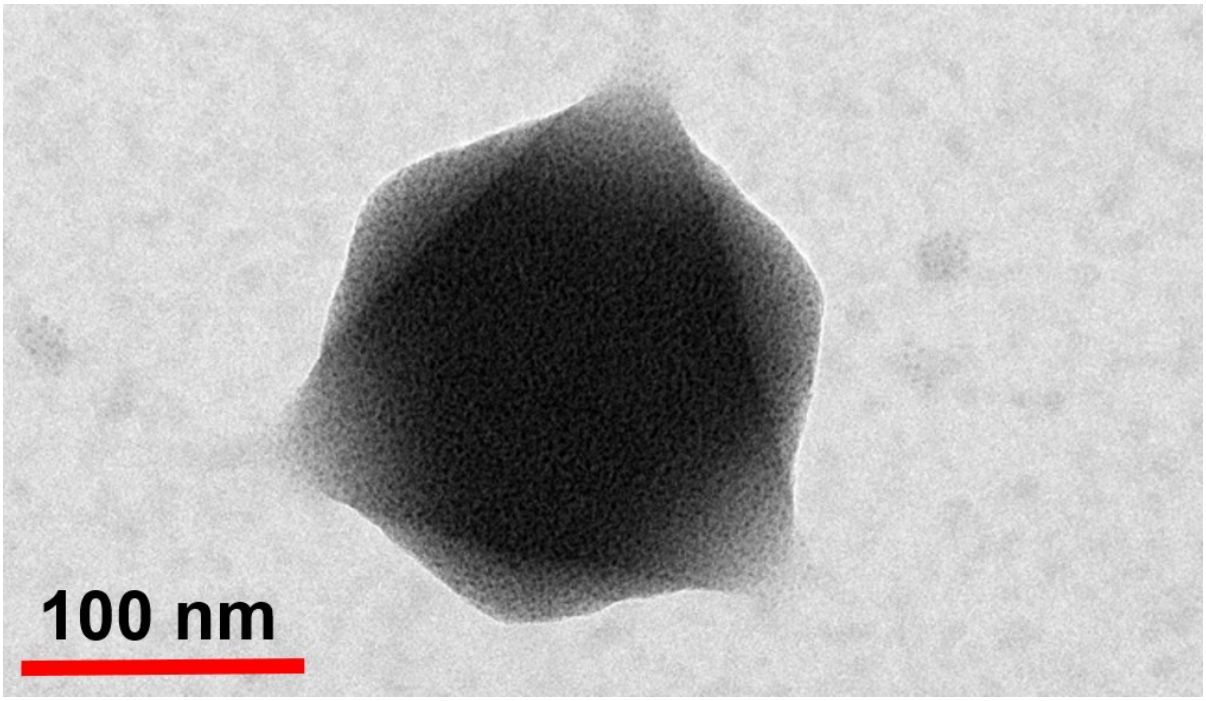

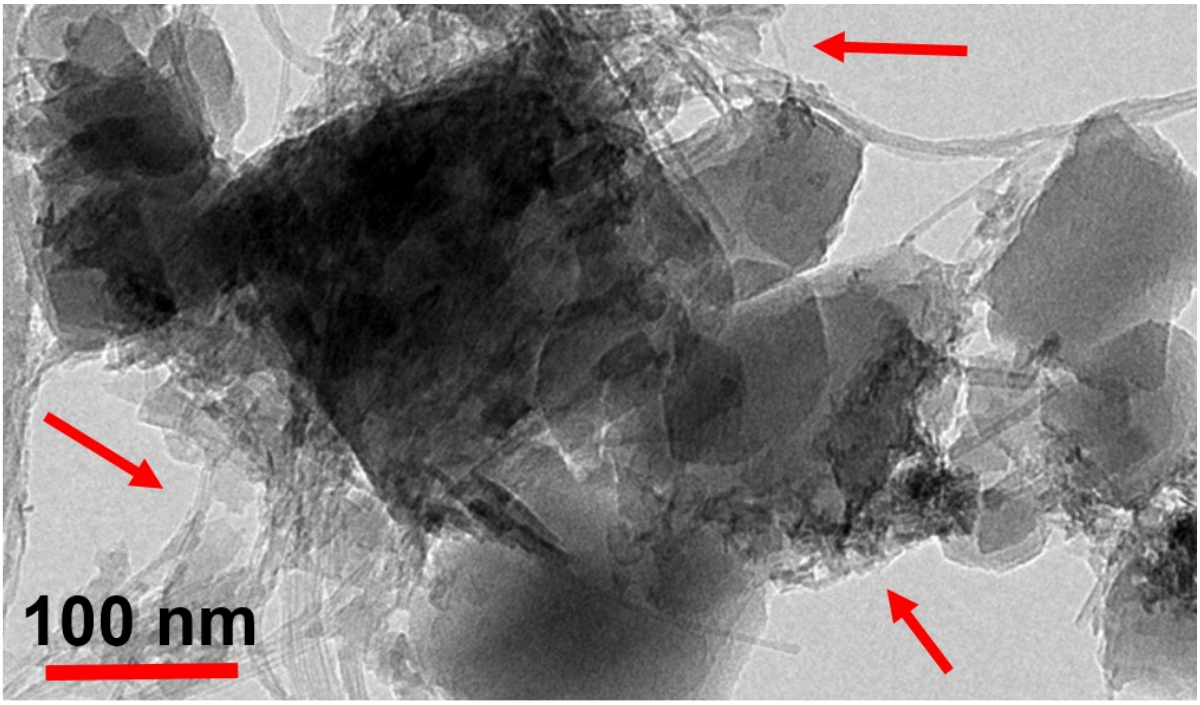

Red arrows indicate points of MWCNT agglomeration.

4. PXRD patterns of pristine and functionalized MWCNTs

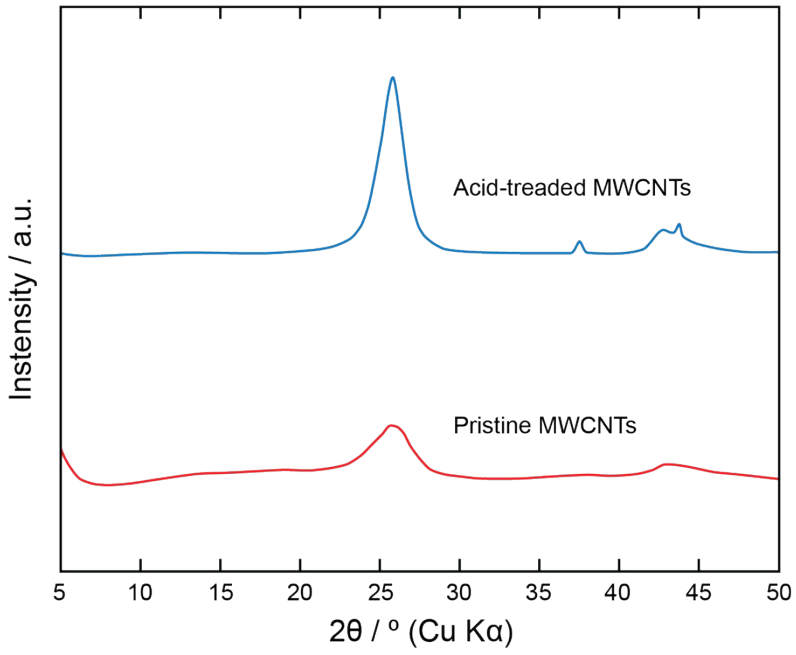

Fig. S1 PXRD patterns for pristine and acid-treated MWCNTs.

5. FTIR spectra of pristine and acid-treated (functionalized) MWCNTs

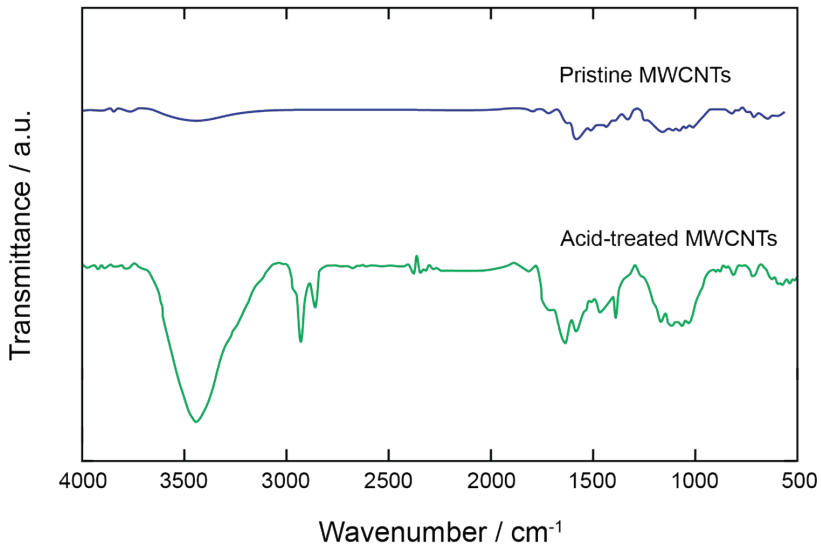

Fig. S2 FTIR spectra of pristine and acid-treated MWCNTs.

6. Step-wise synthesis of MWCNT/MIL-100(Fe) composite

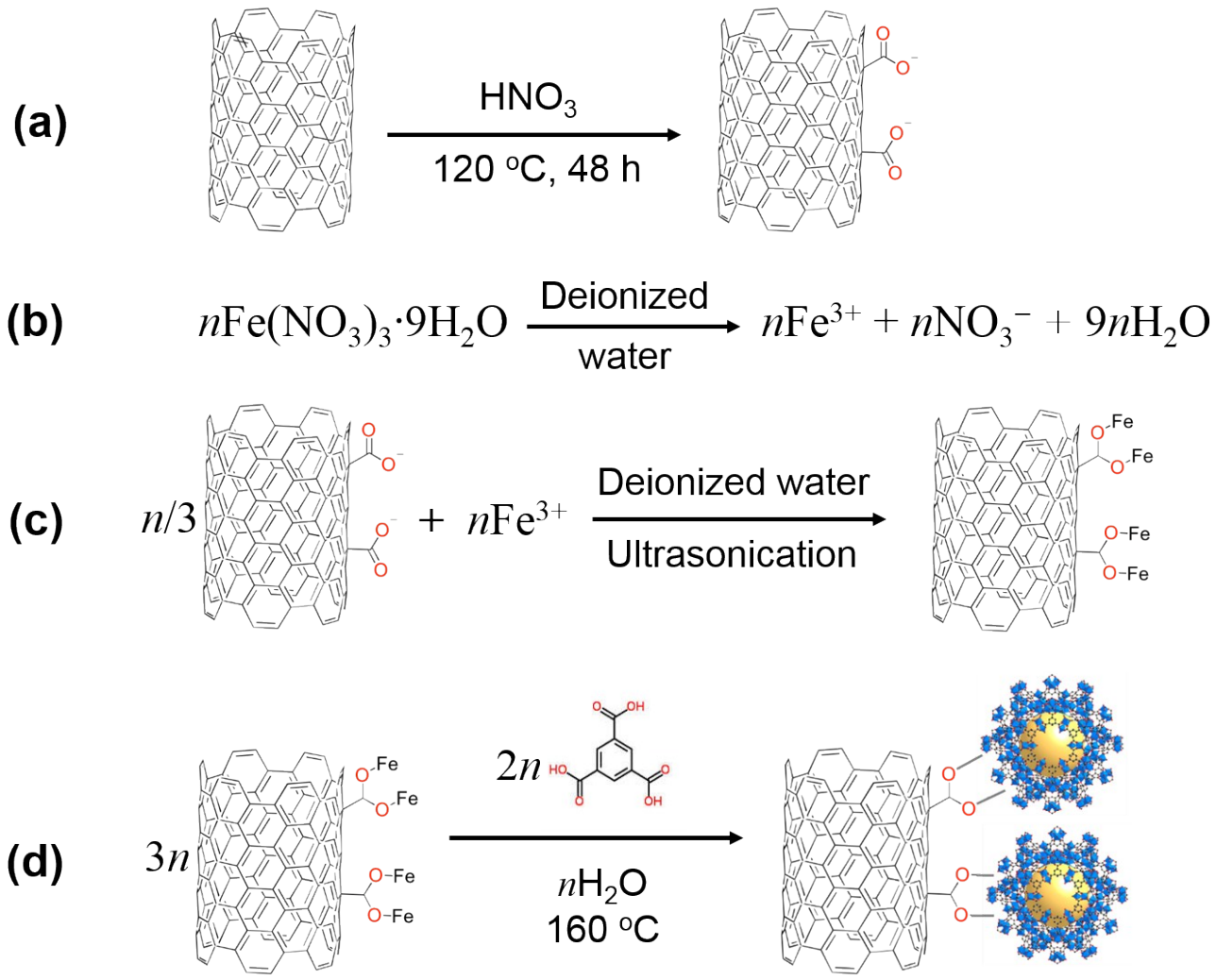

Fig. S3 *In-situ* synthesis of MWCNT/MIL-100(Fe) composite: **(a)** MWCNT carboxylation, **(b)** Dissociation of hydrated Fe-salt in deionized water, **(c)** Molecular-level interaction of negatively charged carboxyl groups on MWCNT and Fe^{3+} ions in aqueous solution, **(d)** Hydrothermal synthesis of MIL-100(Fe) molecules on the surface of MWCNT.

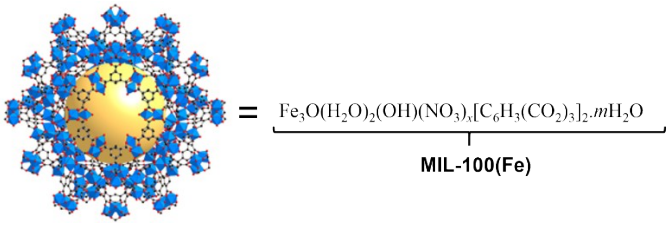

7. Magnified FTIR spectra showing presence of C–O–Fe bonding in MWCNT/MIL-100(Fe) composite.

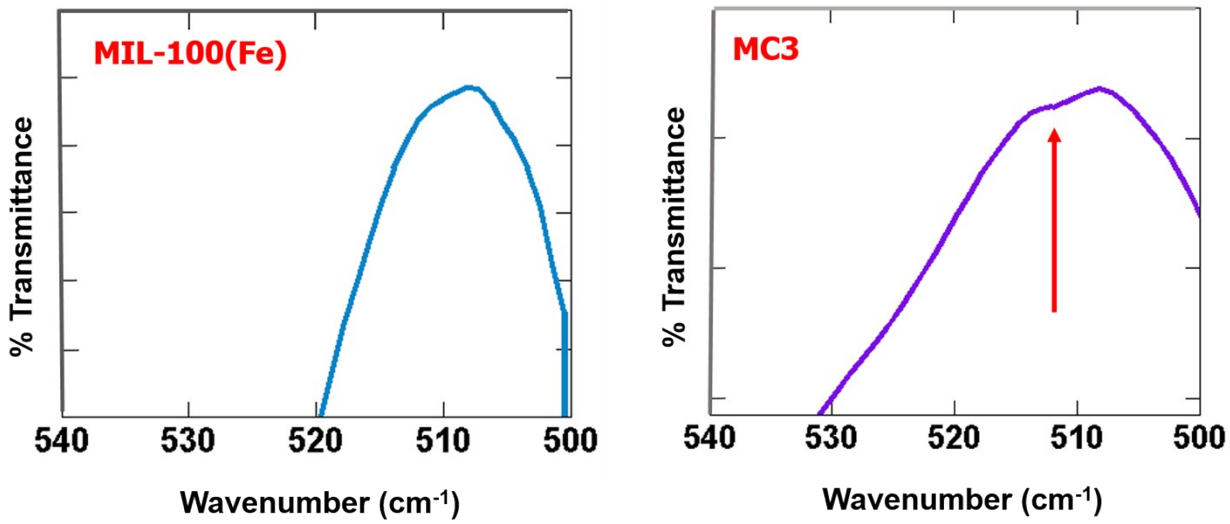

Fig. S4 Magnified FTIR spectra of MIL-100(Fe) and MC3 between 500 and 540 cm^{-1}. Red arrow indicates the existence of C–O–Fe bonding in MWCNT/MIL-100(Fe) composite.

8. XPS spectra of acid-treated MWCNTs, MIL-100(Fe) and MC3

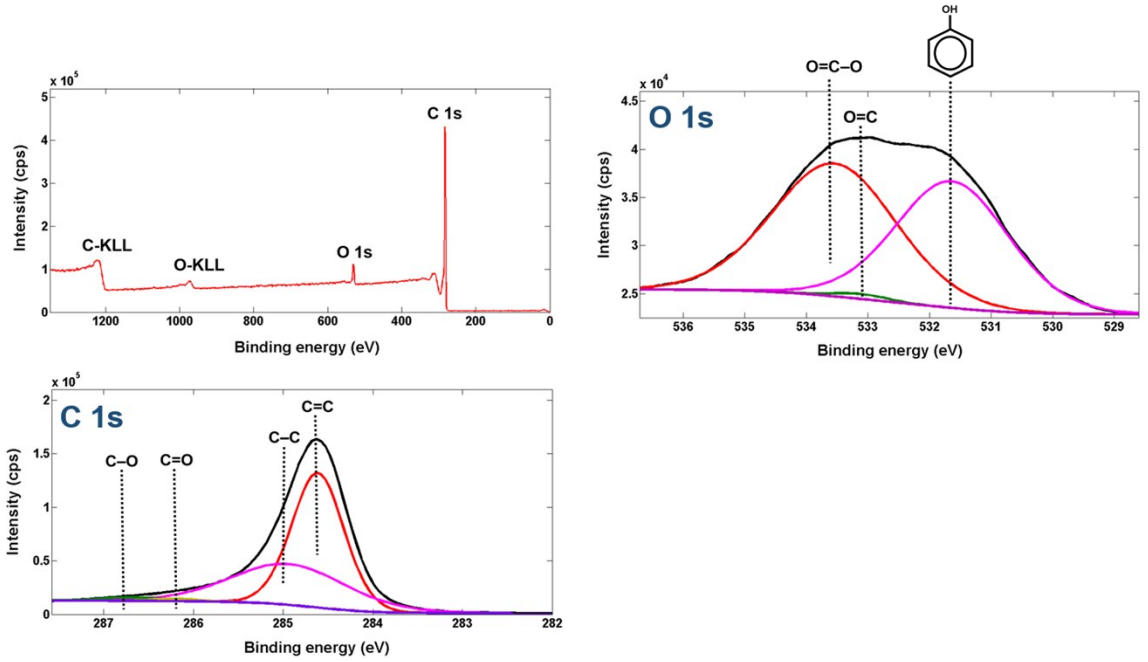

(a)

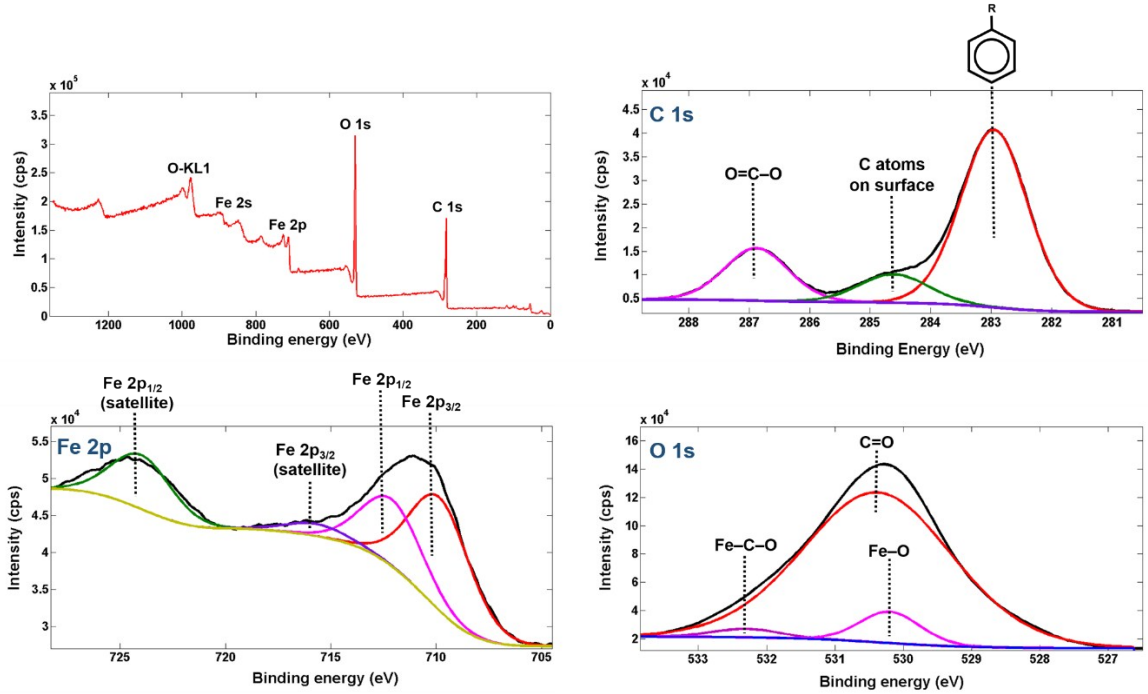

(b)

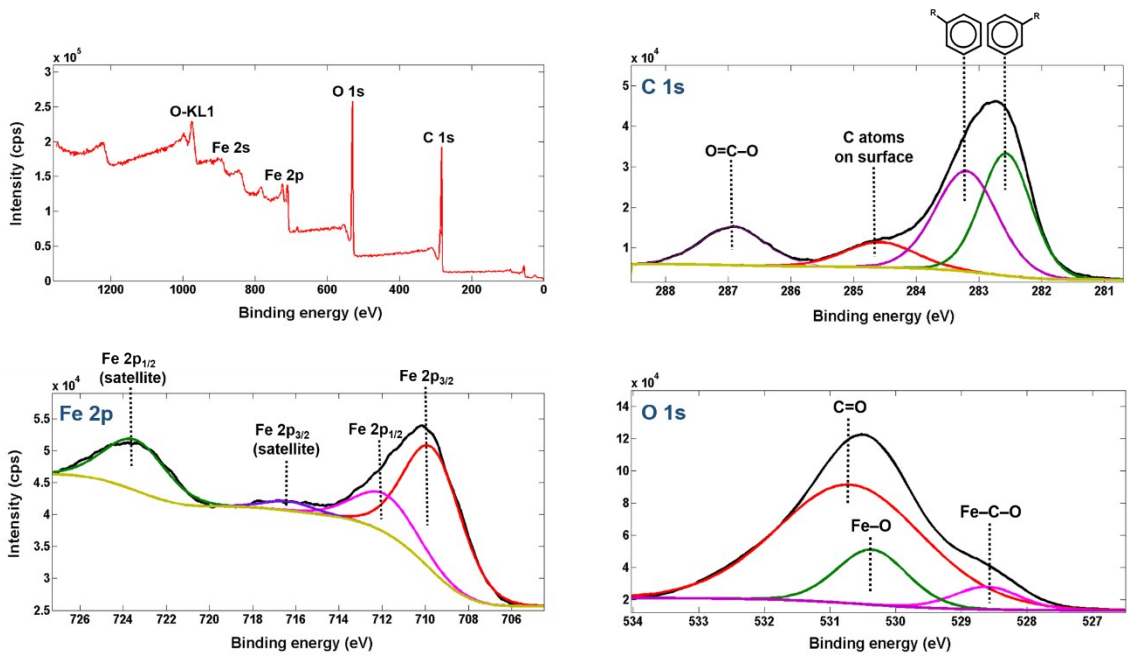

(c)

Fig. S5 XPS spectra of (a) acid-treated MWCNTs, (b) MIL-100(Fe) and (c) MC3.

Table S2. Peak position and intensity data for XPS spectra of acid-treated MWCNTs, MIL-100(Fe) and MC3 (Red entries indicate presence of Fe–C–O bonding between MWCNTs and MIL-100(Fe) crystals in MC3).

	Acid-treated MWCNTs		**MIL-100(Fe)**		**MC3**	
Peak	**Position (ev)**	**Intensity (at.%)**	**Position (ev)**	**Intensity (at.%)**	**Position (ev)**	**Intensity (at.%)**
C1s–A	286.17	0.87	282.95	37.76	283.20	22.78
C1s–B	284.92	37.06	286.88	10.67	286.93	8.99
C1s–C	286.66	1.73	NA	NA	282.57	22.50
C1s–D	284.61	53.27	284.61	6.25	284.58	6.52
O1s–A	531.63	3.30	530.37	38.14	530.69	27.58
O1s–B	533.55	3.62	**532.29**	**0.96**	**528.61**	**2.39**
O1s–C	533.17	0.15	530.20	3.22	530.36	6.19
Fe2p–A	NA	NA	709.83	1.38	709.65	1.66
Fe2p–B	NA	NA	724.01	0.66	723.44	0.73
Fe2p–C	NA	NA	712.12	0.81	711.86	0.55
Fe2p–D	NA	NA	**715.72**	**0.15**	**716.35**	**0.11**

9. SEM micrographs of pristine and acid-treated (functionalized) MWCNTs

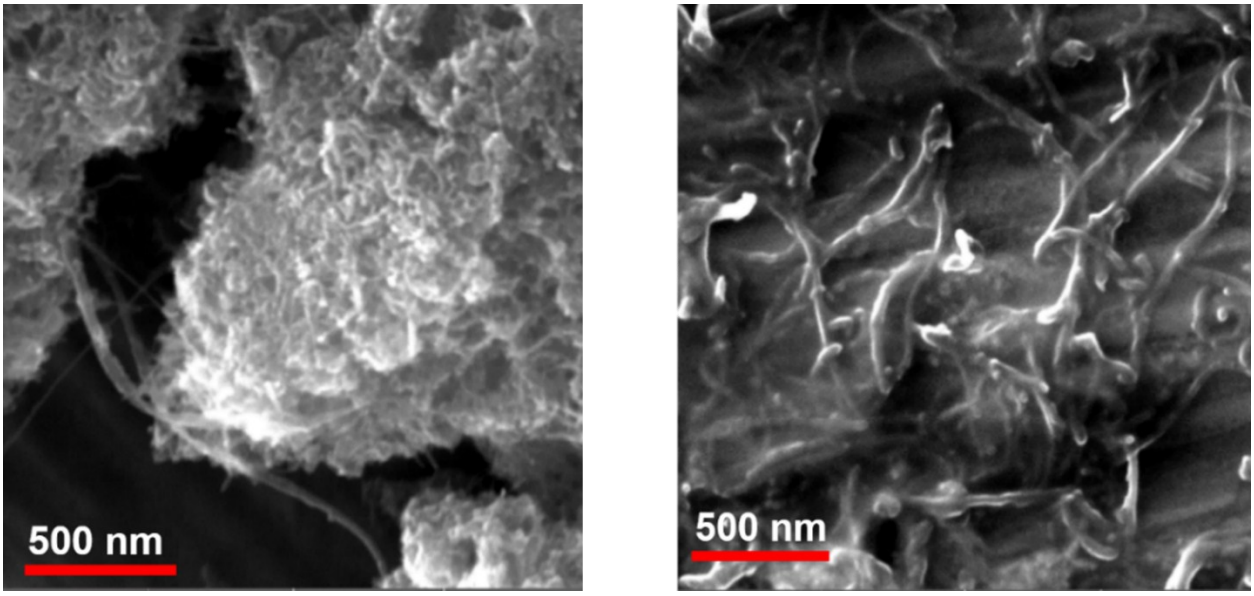

(a) **(b)**

Fig. S6 SEM micrographs of **(a)** pristine MWCNTs, and **(b)** acid-treated MWCNTs.

10. Atomic percentage of each element in MIL-100(Fe) and MWCNT/MIL-100(Fe) composites using EDS analysis and formula unit.

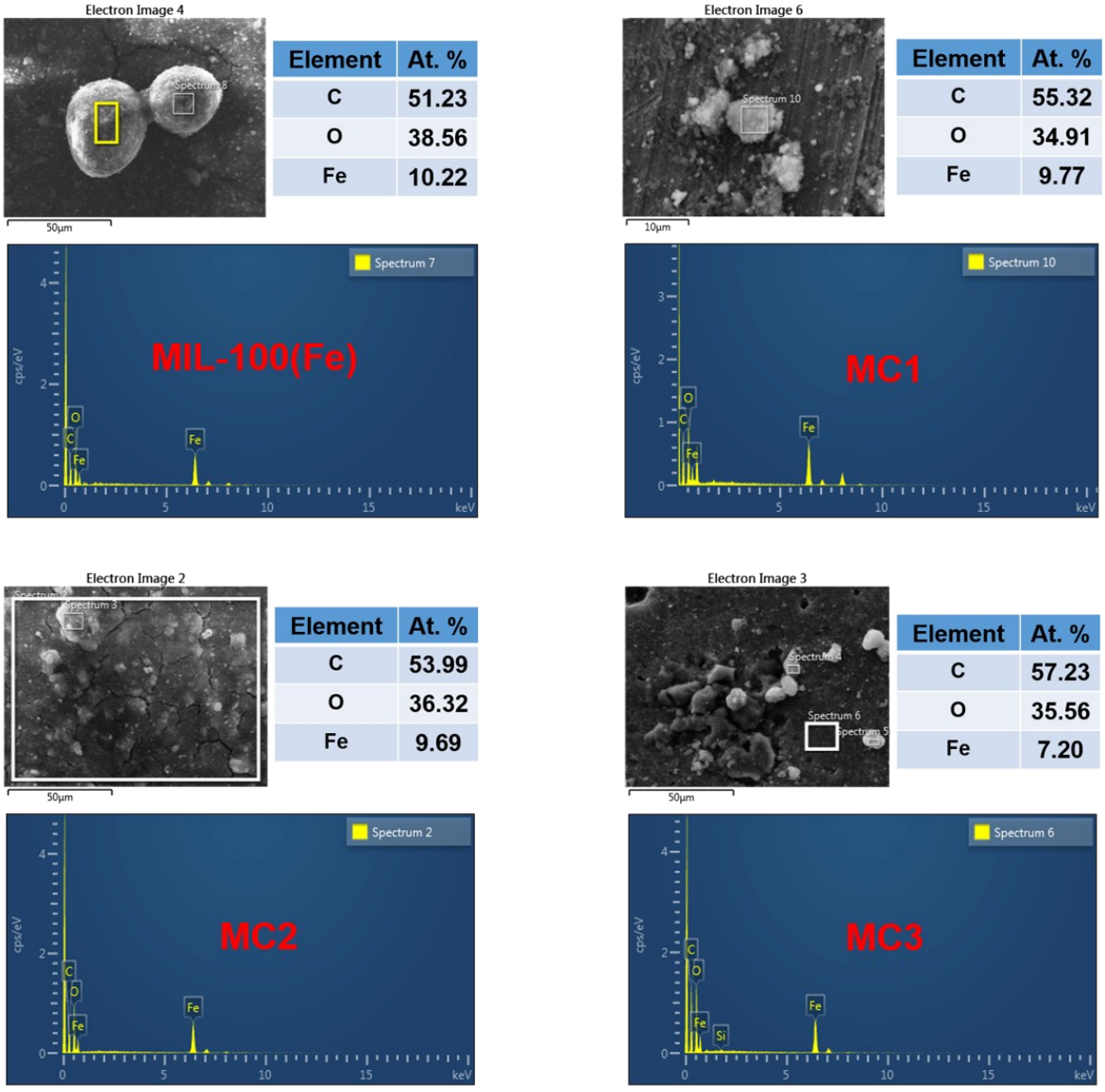

Fig. S7 EDS spectra and atomic percentages of Fe, C, and O in MIL-100(Fe) and MWCNT/MIL-100(Fe) composites.

Table S3 – Comparison of MWCNT content in MWCNT/MIL-100(Fe) composites calculated using EDS and EA.

Sample ID	EA	EDS
MC1	0.82	3.44
MC2	4.70	2.49
MC3	8.08	7.28

11. PXRD patterns of iron oxide (α-Fe_2O_3) residues recovered after TGA of MIL-100(Fe) and MWCNT/MIL-100(Fe) composites

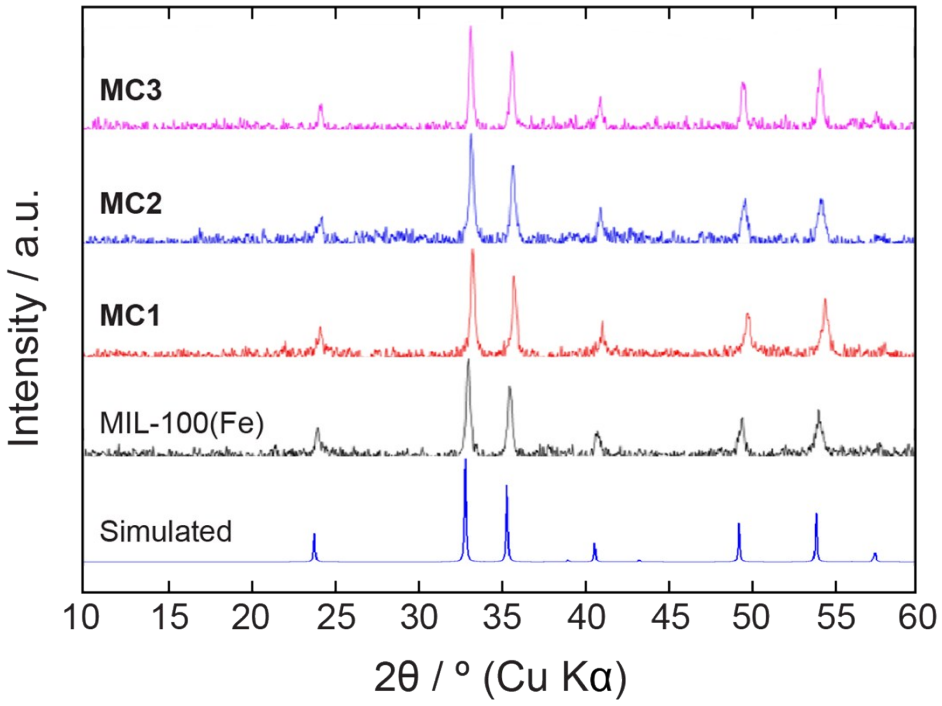

Fig. S8 PXRD patterns of residues recovered after TGA.

12. TGA of acid-treated MWCNTs in air

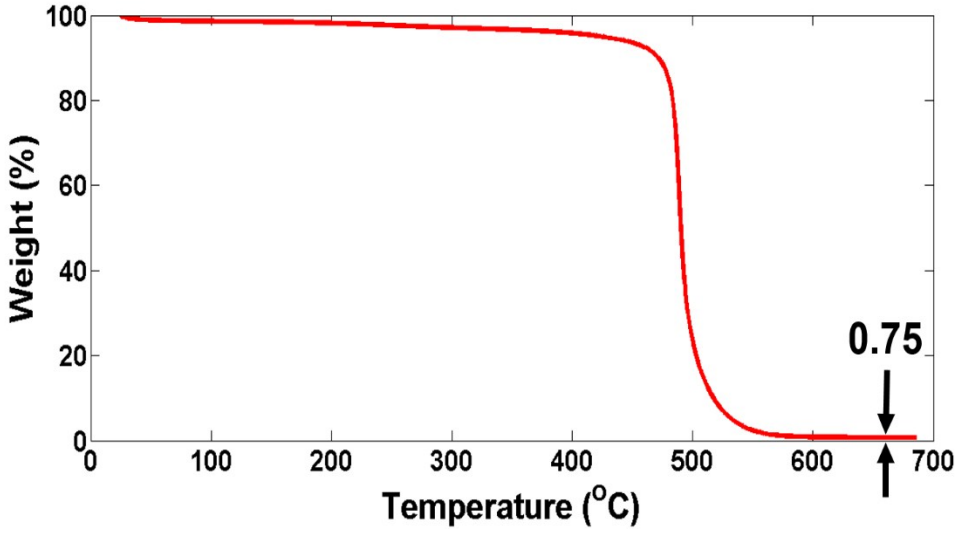

Fig. S9 TGA of acid-treated (functionalized) MWCNTs in air.

13. Calculation of specific heat capacity using DSC data

The specific heat capacity, C_p, can be calculated as [S2]:

$$C_p = \frac{DSC_{sample} - DSC_{baseline}}{DSC_{reference} - DSC_{baseline}} \bullet C_{p,reference} \quad \text{(S2)}$$

where C_p is the specific heat capacity at temperature T, and $C_{p,reference}$ is the specific heat of the standard material (sapphire).

14. Comparison of adsorption isotherms at 298 and 313 K

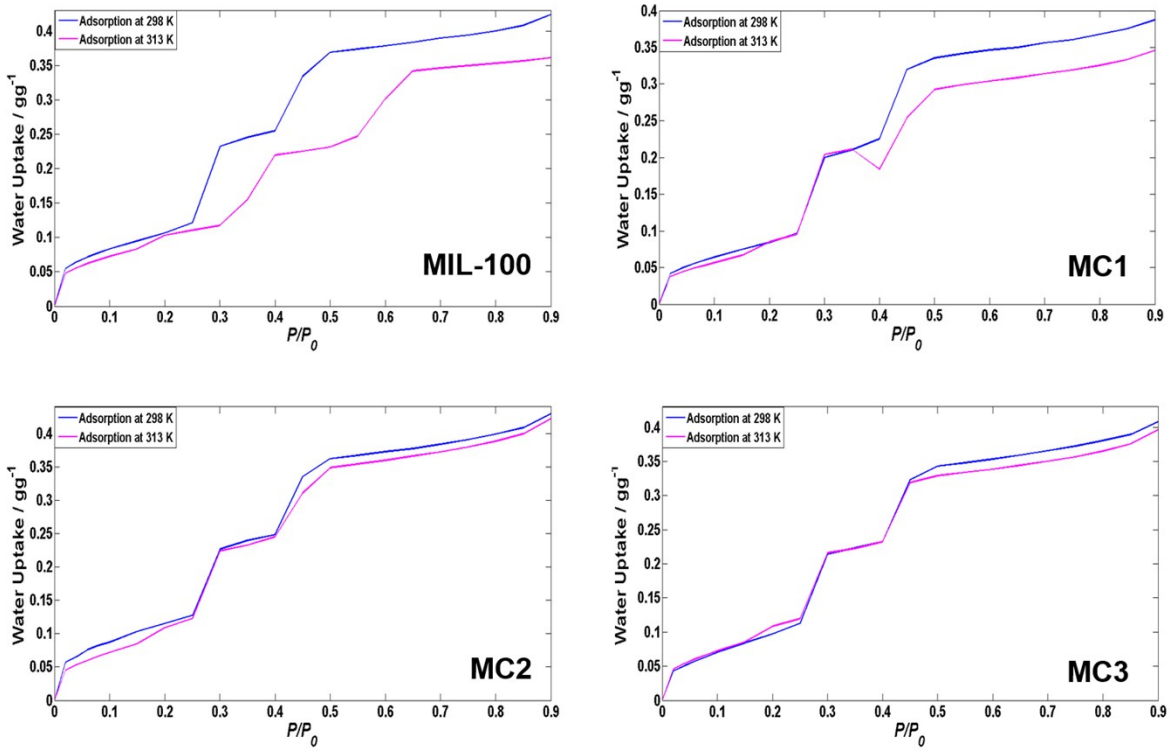

Fig. S10 Water adsorption isotherms at 298 and 313 K.

15. Calculation of differential isosteric heat of adsorption

The average isosteric enthalpy of adsorption ($Q_{st,ads}$) can be expressed as [S3]:

$$Q_{st,ads} = \frac{1}{q_{high} - q_{low}} \int_{q_{low}}^{q_{high}} Q_{st,ads,diff}(q)dq \quad \text{(S3)}$$

where q_{low} and q_{high} denote the lower and upper limits of instantaneous water uptake respectively, while the differential isosteric heat of adsorption $Q_{st,ads,diff}$ can be expressed as [S4]:

$$Q_{st,ads,diff} = -R \ln\left(\frac{p_2}{p_1}\right)\left(\frac{T_1 T_2}{T_2 - T_1}\right) \tag{S4}$$

where p_1 and p_2 are the relative pressures corresponding to $q_{low} \le q \le q_{high}$ for the isotherms measured at temperatures T_1 and T_2 respectively. Hence, for a range of q values, a plot of $Q_{st,ads,diff}$ versus q can be obtained.

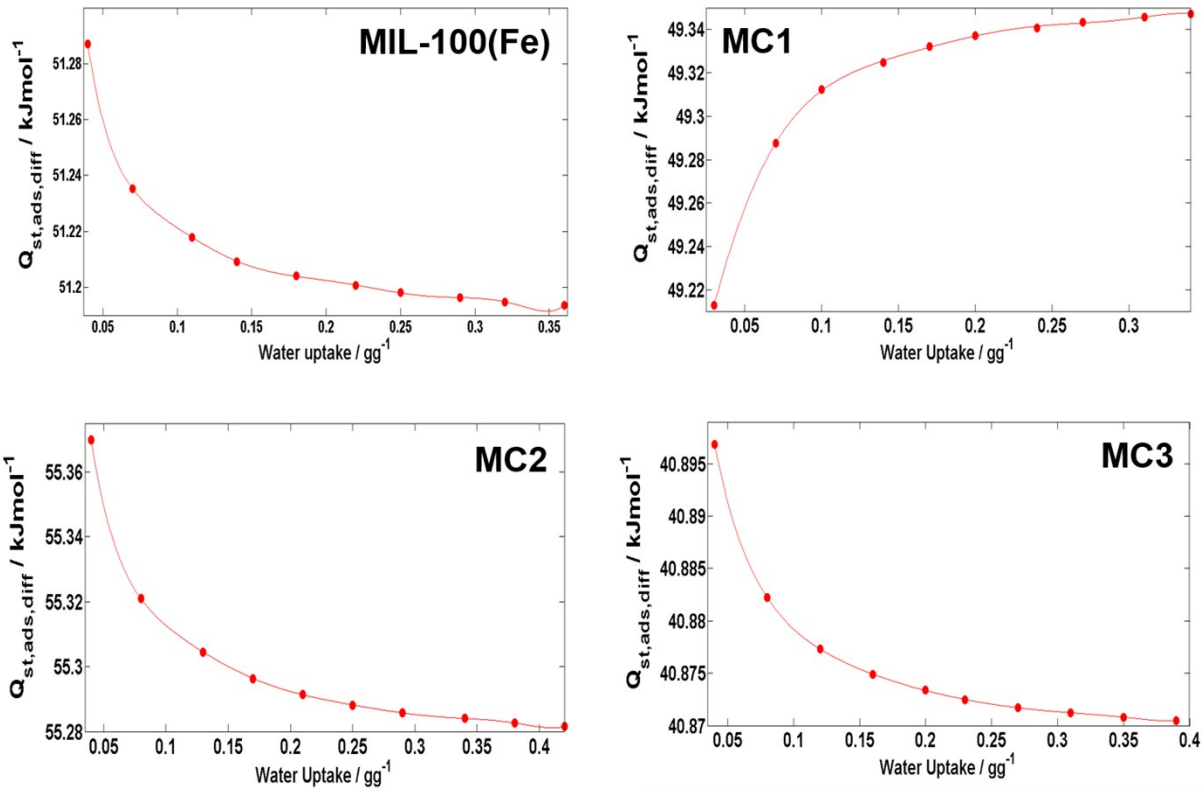

Fig. S11 Variation of differential isosteric heat of adsorption with instantaneous water uptake.

16. Steps to calculate the power capability (*P.C.*) for MIL-100(Fe) and MWCNT/MIL-100(Fe) composites (MC1, -2, and -3)

a. Find which of the four materials shows highest percentage adsorbed amount, q^*, at the end of cyclic adsorption/desorption test.

b. Find the minimum number of cycles, N^*, which each of the other three materials require to reach q^*.

c. Calculate the differential isosteric enthalpy of adsorption $Q_{st,ads,diff}$ for each material at q^*.

d. The power capability (*P.C.*) can now be estimated as:

$$P.C. = \frac{N^* Q_{st,ads}}{T_{tot}} \qquad \text{(S5)}$$

where T_{tot} represents the total time elapsed during the cyclic adsorption/desorption test.

Table S4. Details for calculation of power capability for MIL-100(Fe) and MWCNT/MIL-100(Fe) composites (q^* = 26.1% for **MC1**)

Sample ID	$Q_{st,ads}$ (kJmol^{-1})	N^*	T_{tot} (sec.)	*P.C.* (Wkg^{-1})
MIL-100(Fe)	51.19	12.22	5.1194×10^5	1.03
MC1	49.32	21	5.1480×10^5	1.78
MC2	55.32	11.4	5.12655×10^5	1.28
MC3	40.88	14	5.15115×10^5	1.33

17. Correlation between amount of residual water retained after desorption and isosteric heat of adsorption for MIL-100(Fe) and MWCNT/MIL-100(Fe) composites

Table S5. Correlation between amount of residual water retained inside the pores at the end of single-cycle adsorption-desorption at 298 K, and $Q_{st,ads}$ for MIL-100(Fe) and MWCNT/MIL-100(Fe) composites.

Material	**Residual water at the end of single-cycle adsorption-desorption at 298 K (%)**	$Q_{st,ads}\ \left(\mathbf{kJmol^{-1}}\right)$
MIL-100(Fe)	3.02	51.19
MC1	1.95	49.32
MC2	3.10	55.32
MC3	0.51	40.88

18. SEM micrographs of MIL-100(Fe) and MWCNT/MIL-100(Fe) composites before and after cyclic adsorption-desorption

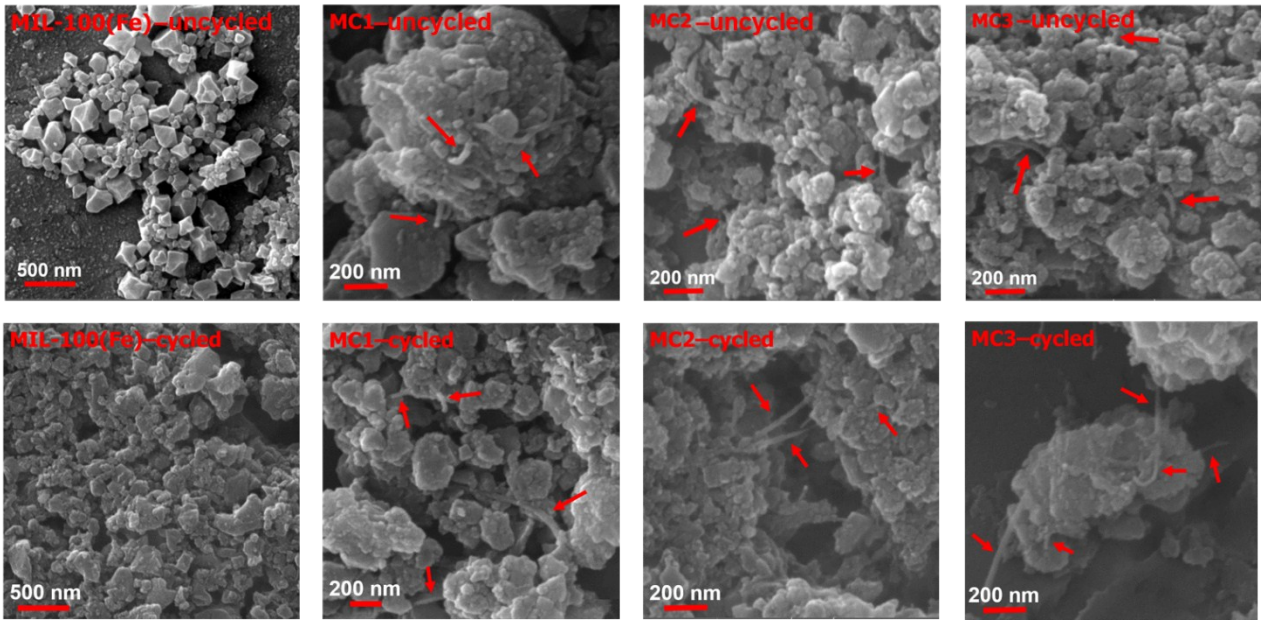

Fig. S12 SEM micrographs of MIL-100(Fe) and MWCNT/MIL-100(Fe) composites before and after cyclic adsorption-desorption tests (red arrows indicate presence of MWCNTs).

19. PXRD profiles of MIL-100(Fe) and MWCNT/MIL-100(Fe) composites before and after cyclic adsorption-desorption

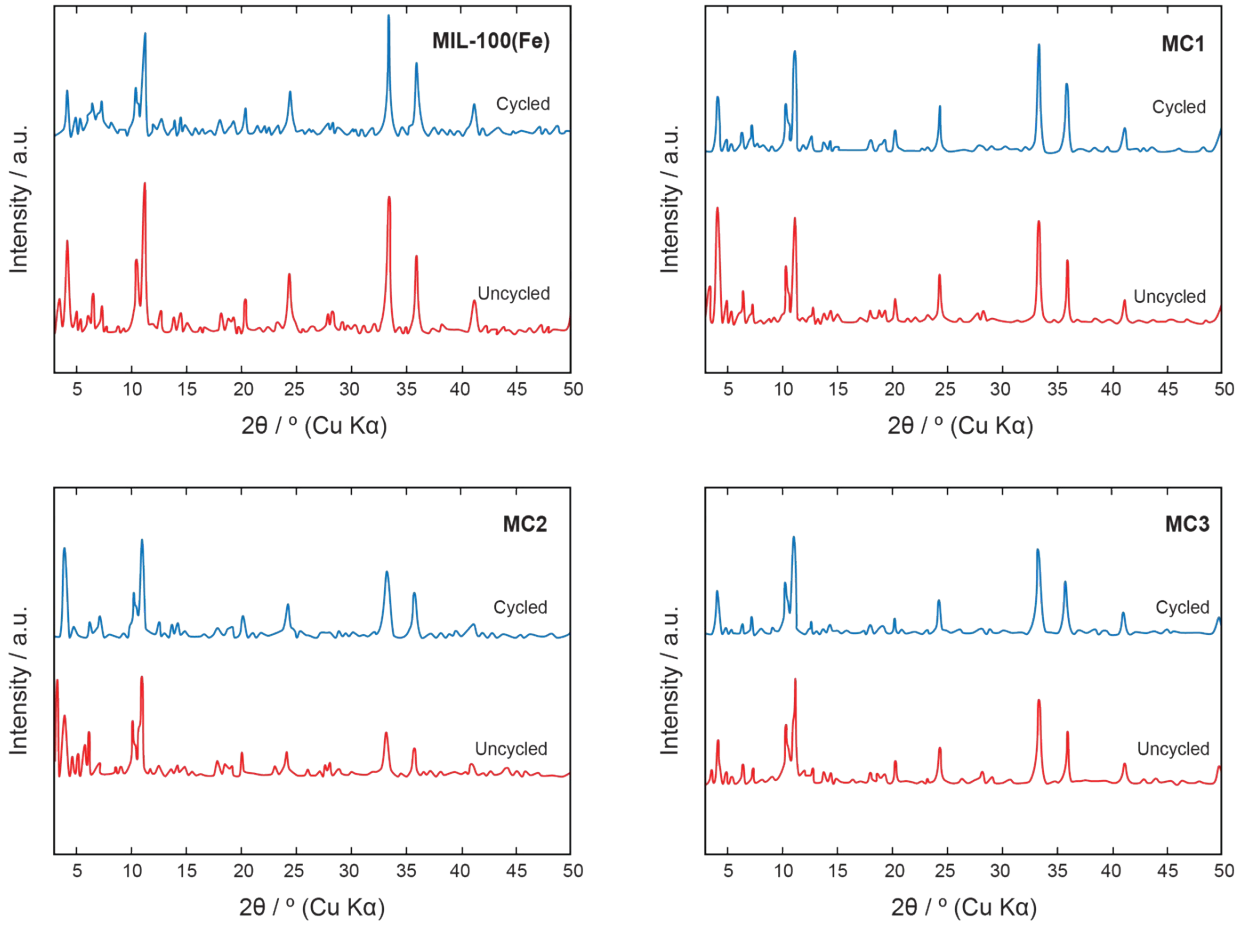

Fig. S13 PXRD patterns for MIL-100(Fe) and MWCNT/MIL-100(Fe) composites before and after cyclic adsorption-desorption tests.

Supporting Information References

[S1] Y. -K. Seo, J. W. Yoon, J. S. Lee, U. -H. Lee, Y. K. Hwang, C. -H. Jun, P. Horcajada, C. Serre and J. -S. Chang, *Microporous Mesoporous Mater*., 2012, **157**, 137.

[S2] B. Mu and K. S. Walton, *J. Phys. Chem. C*., 2011, **115**, 22748.

[S3] F. Jeremias, V. Lozan, S. K. Henninger and C. Janiak, *Dalton Trans*., 2013, **42**, 15967.

[S4] F. Jeremias, A. Khutia, S. K. Henninger and C. Janiak, *J. Mater. Chem.*, 2012, **22**, 10148.